In-situ characterization of thermomechanical behavior of copper nano-interconnect for 3D integration

Bassel Ayoub, Stéphane Moreau, Sandrine Lhostis, Hélène Frémont, Sébastien Mermoz, Emeline Souchier, Emilie Deloffre, Stéphanie Escoubas, Thomas W Cornelius, Olivier Thomas

In-situ Characterization of Thermomechanical Behavior of Copper Nano-Interconnect for 3D Integration

B. Ayoub[1,2,3,a)], S. Moreau[2], S. Lhostis[1], H. Frémont[3], S. Mermoz[1], E. Souchier[1], E. Deloffre[1], S. Escoubas[4], T. W. Cornelius[4], O. Thomas[4]

[1)]STMicroelectronics, 850 rue Jean Monnet, 38926 Crolles Cedex, France.
[2)]Univ. Grenoble Alpes, CEA, LETI, 38000 Grenoble, France.
[3)]IMS Laboratory, University of Bordeaux, UMR 5218, 33405 Talence, France.
[4)]Aix-Marseille Université, Université de Toulon, CNRS, IM2NP, Marseille, France.
[a)]Author to whom correspondence should be addressed: bassel.ayoub@st.com

Abstract – Hybrid bonding is a very promising 3D packaging technology which allows extremely high interconnect density between electronic chips. In its most advanced interconnect pitch, Cu pads as small as 300 nm may be used. Successful bonding relies directly on the thermomechanical displacement of Cu above the oxide matrix. Hence, the control of this technology relies on a profound understanding of the thermomechanical behavior of 300 nm Cu pads. To achieve this goal, X-ray synchrotron Laue micro-diffraction is used to monitor the strain state and orientation of individual Cu pads *in situ* during heat treatment. The experimental findings are completed with Finite Element Modeling simulations including elastic anisotropy and plastic behavior. The 300 nm Cu pads are found monocrystalline with random lattice orientations. The thermomechanical behavior of each pad is found highly driven by its crystal orientation in accordance with the elastic and plastic anisotropy of copper. Very good agreement is found with simulations offering profound understanding of the single nanocrystalline Cu grains properties and providing solid conclusions for a successful hybrid bonding at sub-micrometric pitch level.

Keywords: Nano-interconnect, Cu/SiO_2 Hybrid Bonding, Laue Microdiffraction, Microstructure, Thermomechanical behavior, Plasticity

1. Introduction

3D heterogeneous integration has been identified as a key enabler for More Moore scaling [1]. The latest generation is Wafer-to-Wafer (W2W) fine pitch hybrid bonding allowing higher density of integration and higher performance [2]. Further scaling down to sub-micron pitch requires material behavior deep understanding. At the sub-micron scale, material properties change significantly from their bulk one and are dependent on grain size [3-5]. The Cu nano-interconnects electrical properties have been widely studied showing increased electrical resistivity with decreased grain size [6]. In addition, a clear impact of size reduction on the electromigration reliability response have been shown [7][8]. For the Cu nano-interconnects dedicated for hybrid bonding, the very first challenge concerns the thermo-mechanical properties since successful bonding is mainly based on Cu displacement that enables interface closure during annealing.

Many studies focused on the Cu mechanical properties at the micro and nano-crystal range. Indeed, tensile tests conducted at room temperature on nanocrystalline Cu demonstrated a near-perfect plastic behavior combined with high plastic flow whereas microcrystalline Cu exhibits the usual work-hardening behavior after yielding [9]. Focusing on nanocrystalline Cu, atomistic simulations evidenced a decreasing yield stress with diminishing grain size, resulting in a reverse Hall–Petch effect [10][11]. As for the hybrid bonding technology, thermo-mechanical simulations revealed that achieving full Cu-Cu connection during annealing becomes more and more difficult with smaller pad width [12]. Aside from the mechanical properties' size dependance, an important consideration for Cu is its crystalline orientation. Cu is known to be elastically highly anisotropic (Zener ratio of 3.2) with a Young's modulus along [111] being three times larger than along the [100] direction. Previous experiments performed on single micrometric Cu crystals clearly evidenced a relation between orientation and yield strength with the [111] orientation having much higher values [13]. However, the thermo-mechanical properties dependence on orientation is still unsolved for Cu crystals with a size ranging between 100 and 1000 nm, which is actually of paramount interest to reach mass production of the sub-micron hybrid bonding pitch.

This paper presents the first in-situ study of the thermomechanical behavior of single nanocrystalline Cu grains by combining Laue micro-diffraction experiments and Finite Element Method (FEM) simulations including Cu anisotropy. It offers profound and unique understanding of the single nanocrystalline Cu grains behavior. Application of this study allows defining the conditions for full bonding at the sub-micrometric hybrid bonding pitch level.

2. Structure and Experimental Procedure Description

As schematically illustrated in Fig. 1(a), the test structure is composed of single non-bonded Cu pads with a diameter of 300 nm, a thickness of ~850 nm and an inter-pad spacing of 2.6 µm ensuring that neighboring pads do not contribute to the recorded diffraction patterns. After Chemical Mechanical Polishing (CMP), a 60 nm layer of SiN was deposited on the top surface to avoid Cu oxidation during the analysis.

White beam Laue microdiffraction was performed at the BM32 beamline of the ESRF in Grenoble (France). The polychromatic x-ray beam with an energy bandwidth from 5 to

25 keV was focused down to a size of 500 nm (H) × 500 nm (V) on the sample surface (which is inclined by 40° with respect to the incident beam) using a pair of Kirkpatrick-Baez mirrors. The diffracted x-rays were recorded by a sCMOS detector (*Photonic Science*) with 2018 × 2016 pixels and a pixel size of 73.4 µm × 73.4 µm which was installed at an angle of 90° with respect to the incident x-ray beam at 77 mm from the sample position. An Anton Paar® furnace was used for in-situ annealing experiments which were conducted at room temperature, at 100 °C and, then in steps of 50 °C up to 400 °C. The heating rate was 15 °C/min with a stabilization time of ~5 minutes at each temperature step. Laue microdiffraction patterns for 10 Cu pads were acquired at each step. At the highest temperature, three acquisitions were recorded to simulate the real bonding annealing duration of 2 hours. The microstructure and deformation were further monitored while cooling down to ambient temperature with a step of 100 °C without controlled cooling rate. The Laue microdiffraction patterns were analyzed using the LaueTools software [14]. This technique gives information about microstructure and deviatoric strain with very high resolution (10^{-4}) [15][16].

Laue microdiffraction only gives access to the deviatoric strain which is mostly related to the change of shape of the unit cell. The hydrostatic part, which is related to volume change and therefore determines the pad's thermal expansion in the present work, is not experimentally accessible [17]. Thus, the full strain tensors were calculated by 3D finite element method (FEM) simulations using COMSOL Multiphysics®. The 3D model bases on a 300 nm single pad embedded in a SiO_2 matrix with 750 µm Si substrate. Symmetric boundary conditions are applied at two sides. The thicknesses of Cu pads and SiO_2 were extracted from Transmission Electron Microscopy (TEM) images. Each pad with its given material properties inferred from Laue microdiffraction was investigated separately by FEM. We used a linear isotropic behavior for both Si and SiO_2. Their corresponding thermoelastic constants (E, ν and α) were taken from literature at ambient temperature [18-20]. For Cu, the elastic anisotropy was included using the elastic constants C_{11} = 168.4 GPa, C_{12} = 121.4 GPa, and C_{44} = 75.4 GPa which were taken from ref. [21]. The rotation matrix for Cu pads was defined by taking the Euler angles inferred from Laue microdiffraction for each pad.

3. Data/Results and Discussion

3.1 Experimental Results

Laue micro-diffraction patterns from one row of Cu pads (Fig. 1(b)) were indexed revealing that each pad consists of a single grain suggesting that they are either monocrystalline or that there is a dominant grain in each pad. Among the 10 analyzed Cu pads, no dominant orientation was evidenced as shown in Fig. 1(c). When heating up to 400 °C, the grain orientation remains unchanged.

Because copper is a very elastically anisotropic material, this spread in orientation has direct consequences on the elastic behavior of different pads. Based on the hkl Miller indices, the Young's modulus along Z was calculated using equation (1) considering the elastic constants mentioned above [22]:

$$\frac{1}{E_{uvw}} = \frac{C_{11}+C_{12}}{(C_{11}-C_{12})(C_{11}+2C_{12})} - 2\left[\frac{1}{(C_{11}-C_{12})} - \frac{1}{2c_{44}}\right](u^2v^2+v^2w^2+w^2u^2) \quad (1)$$

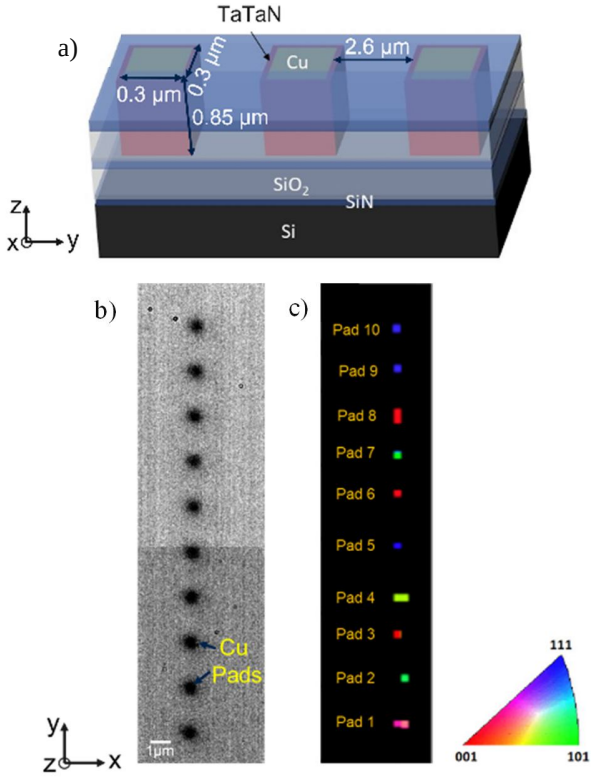

Fig. 1. (a) 3D schematic illustration of the sample used for in-situ measurements with temperature, (b) top view using optical microscopy showing the 10 Cu pads and (c) the corresponding Inverse Pole Figure (IPF) orientation map in Z.

The u, v and w are the direction cosines of the investigated direction. The calculated Young's moduli for all pads measured in this work are presented in Table 1. The Young's modulus varies between 68 and 198 GPa depending on the grain orientation. It is thus expected that these different pads will have different thermoelastic behaviors. The analysis of the deviatoric strain focuses on the deformation along Z since it is directly related to interface closure after annealing. At 30 °C, a negative deviatoric strain is observed for all pads with the modulus of the strain being the larger the lower the Young's modulus as shown in Fig. 2(a). One Cu Pad with 130 GPa Young's modulus has lower deviatoric strain than the two neighboring points which is mostly related to different strain free temperature.

TABLE 1. hkl Miller indices and Young's Modulus for the 10 Cu pads

Pad Number	Orientation along Z			Young's Modulus along Z (GPa)
	h	k	l	
1	1	0.6	0.37	127
2	1	0.76	0.24	130
3	1	0.1	0.02	68
4	1	0.9	0.6	169
5	1	0.89	0.87	188
6	1	0.24	0.47	102
7	1	0.85	0.56	164
8	0.7	1	0.2	132
9	1	0.56	1	172
10	1	1	0.9	198

The deformation after an annealing time of 2 hours at 400 °C is presented in Fig. 2(b). For the sake of clarity, only the results for pads with the lowest and the highest Young's modulus are shown. For the pad with the largest Young's modulus along Z (pad 10, 198 GPa), the deviatoric strain increases linearly from room temperature up to 400 °C. In contrast, the grain with the lowest Young's modulus (pad 3, 68 GPa) shows a clear deviation from the linear relationship for T < 150 °C and T > 350 °C which might be related to plastic deformation. This behavior is observed for all pads with E smaller than 130 GPa. The strain free temperature, which was extracted from the experimental curves in Fig. 2(b), varies between 250 °C and 300 °C for all pads. After cooling down to 30 °C, the strain is different from the initial value which is an indication for plastic deformation or a microstructural evolution. The variation of the deviatoric strain at 400 °C in comparison to the initial value at 30 °C is displayed in Fig. 2(c) revealing that ε_{dev} varies the most the smaller the Young's modulus is. Thus, Cu pads with an orientation that has a smaller elastic constant along Z exhibits a larger deformation.

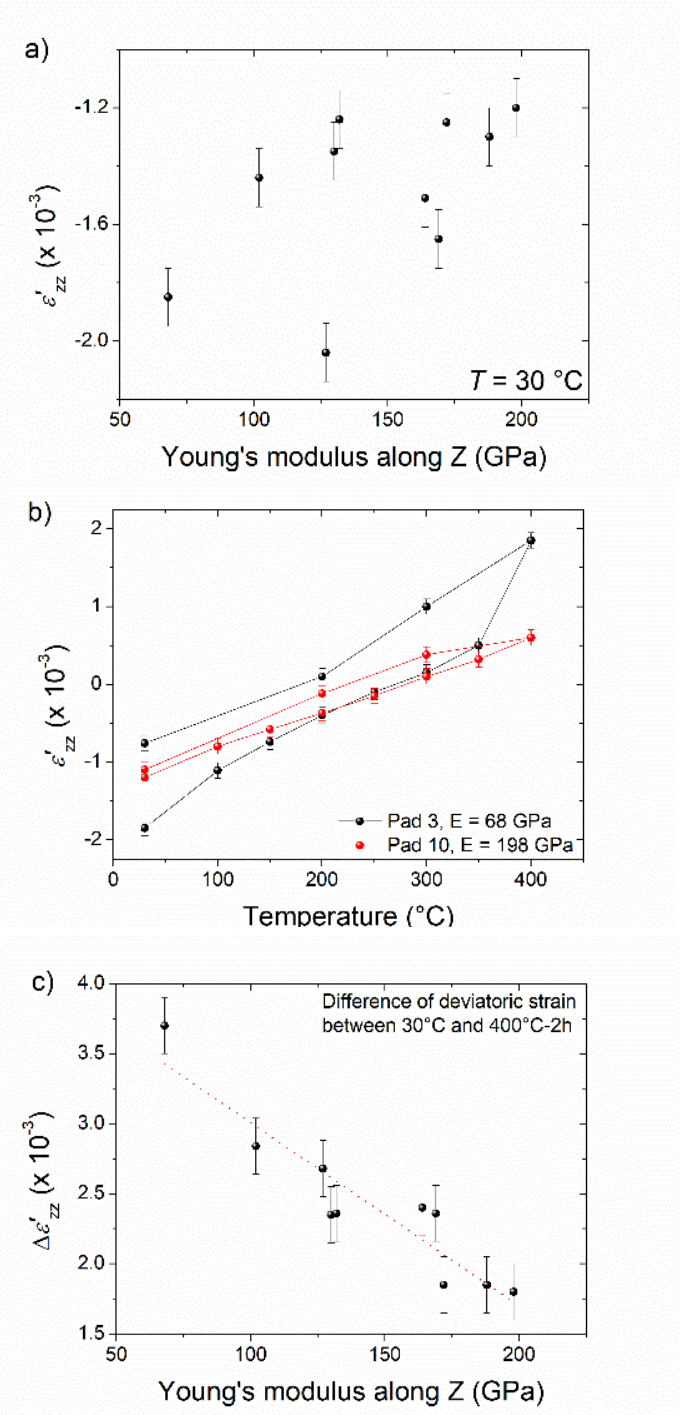

Fig. 2. (a) Deviatoric strain at 30 °C vs. Young's modulus for all the pads. (b) Deviatoric strain vs. temperature for the pads with the lowest E value (pad 3) and the highest E value (pad 10). (c) The delta of deviatoric strain between 30 °C and 400 °C vs. Young's modulus for all Cu pads. Vertical bars represent the experimental uncertainty.

3.2 Numerical Simulations Results

While Laue microdiffraction gives access only to the deviatoric strain, the full strain tensor was computed by finite element method simulations. An important parameter to define is the temperature at which the pad does not exhibit any thermal strain. This strain-free temperature was taken from the experimental curves. For all the pads, simulations reproduced the linear trend and the slope of the experimental curve distinguishing two different behaviors. For pads with E>130 GPa, simulation and experiment agree very well with each other as illustrated exemplarily for pad 10 in Fig. 3(a).

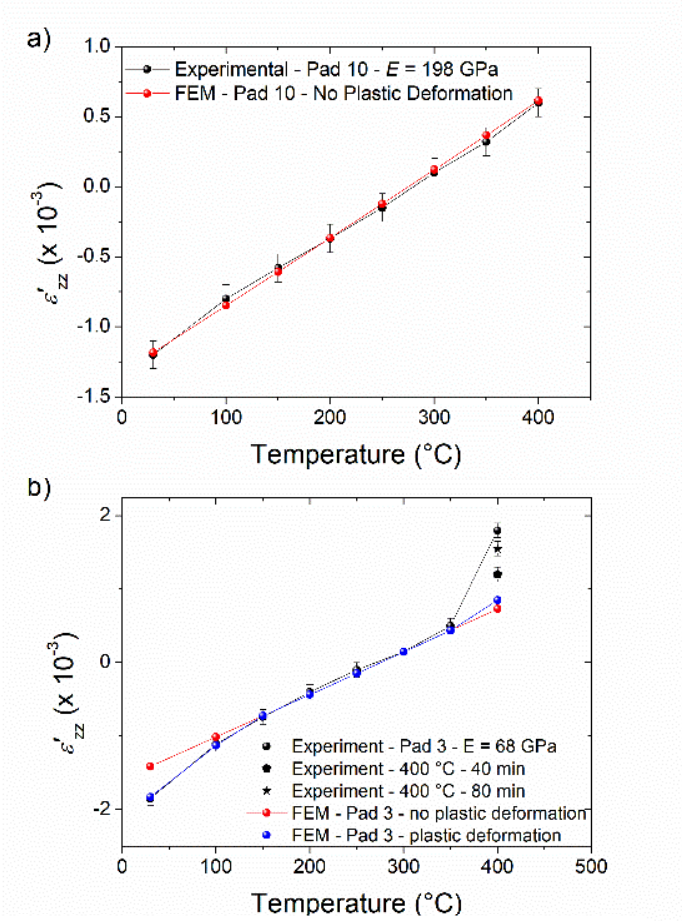

Fig. 3. Comparison between experimental and FEM simulations results for the pads with (a) the lowest E value (pad 3) and (b) the highest E value (pad 10). Vertical bars represent the experimental

However, for pads with E<130 GPa, the fully elastic simulation fails to reproduce the nonlinear experimental behavior for T<150 °C and for T > 350 °C as shown in Fig. 3(b) for pad 3. This clearly indicates the need to include plasticity in the simulation.

In order to account for plasticity within the FEM simulations, a Ludwick power model is adapted which is given by equation (3):

$$\sigma = \sigma_y + K\varepsilon_p^N \quad (3)$$

Here σ_y is the yield stress in MPa, K is the strength coefficient in MPa, ε_p is the plastic strain and N is the stress exponent. A Design of Computer Experiments (DoCE) mixing Central Composite Design (CCD) and Latin Hypercube Sampling (LHS) was designed. The range of variations are the following: 100-400 MPa for the yield strength σ_y, 100-3000 MPa for the strength coefficient K and 0.1-0.9 for the stress exponent N. A total of 70 runs were performed. This DoCE is applied at two different temperatures (30 °C and 100 °C) for each pad exhibiting a shift between numerical and experimental trends. For a given temperature, numerous combinations of parameters exist giving the same response as the experimental one. However, the number of combinations can be strongly restricted by fitting the complete range from room temperature to 100 °C. For pad 1 (E=127 GPa), σ_y was found to fit between 180-190 MPa, K between 650-700 MPa and N between 0.35-0.4 while for pad 2 (E=130 GPa), σ_y fits between 185-189 MPa, K between 670-720 MPa and N between 0.3-0.37. For pad 3 (E=68 GPa), σ_y was found to fit between 140-146 MPa, K between 650-700 MPa and N between 0.65-0.72 while for pad 6 (E=102 GPa), σ_y fits between 160-170 MPa, K between 700-725 MPa and N between 0.55-0.6. The results indicate that the yield stress σ_y increases with increasing E. The Schmid factor decreases when tending to the [111] orientation leading to higher yield stress. This explains why no plastic deformation is observed on Cu pads with E > 130 GPa. Previous studies performed on much larger single crystals also showed a relation between orientation and σ_y [13]. As for the stress exponent N, it has an opposite behavior to σ_y where it increases with decreasing E. The strength coefficient K does not seem to vary with E. The parameters N and K were previously reported for annealed Cu to be 0.54 and 315 MPa, respectively [23]. In addition, recent nanoindentation measurement on Cu grains with a size of 1 µm revealed a strength coefficient K of 1600 MPa, a yield strength σ_y ranging from 200 to 300 MPa, and N between 0.2-0.3 [24]. These studies, however, did not consider the crystalline orientation which may explain the differences with the values reported in the present work.

Excellent agreement of the simulated behavior with the experimental behavior is obtained at 30 °C and 100 °C when adding plasticity to the computations as shown in Fig. 3(b) for the pad 3. However, the model cannot reproduce the deviatoric strain evolution at 400 °C. The deviatoric strain evolution was monitored at 400 °C by consecutive Laue microdiffraction during the 2h annealing period revealing an increasing ε'_{zz} with increasing time as shown in Fig. 3(b). This creep behavior is observed only for pads with E < 130 GPa. In general, creep typically occurs for metals at temperatures on the order of half of the melting temperature (for Cu the creep temperature is around 400 °C). Considering the limited number of Cu grains studied experimentally, the exact parameters and the exact creep behavior (Nabarro-Herring, Norton, Garofalo…) cannot be determined. In addition, creep also plays a significant role on the hydrostatic part of the stress i.e., the deviatoric part obtained experimentally is not sufficient to estimate the full strain tensor.

Based on the excellent agreement between calculated and measured deviatoric strains, one can rely on the calculated total stress and strains. The total stress (deviatoric + hydrostatic stresses) and the deviatoric stress were studied as a function of the temperature by FEM simulations considering the experimentally determined deviatoric stress and grain orientation. An example is shown in Fig. 4 for the pad 3. The total stresses along X, Y and Z at the Cu pad level are tensile at 30 °C. This is explainable since the coefficient of thermal expansion (CTE) of Cu is much larger than the ones of SiO_2 and Si. Therefore, when the structure is cooled down from elevated deposition temperature to room temperature, the CTE mismatch of Cu and the substrate leads to the thermally induced tensile stress [25][26]. The total stress level is higher in X and Y directions than in the Z direction because the pad is free to relax vertically. When heating the sample, the total stresses decrease with increasing temperature until reaching the stress-free state at T ~ 275 °C and then changing sign leading to Cu pads which are in compression. As for the deviatoric part in Z, it is compressive at 30 °C for all the pads. This explains the negative deviatoric strain observed both by FEM simulation and experimentally. This time, the absolute deviatoric stress state is larger along Z than in the other directions meaning that a larger part of the total stress originates from the deviatoric one.

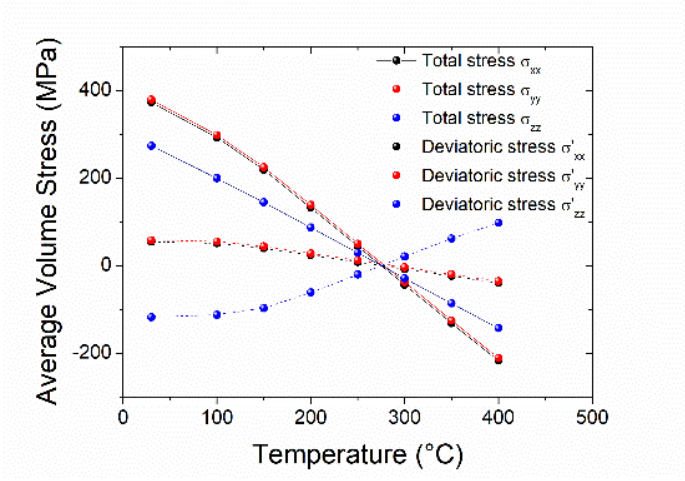

Fig. 4. Average volume results of the total and deviatoric stresses as a function of temperature for the pad with the lowest E value (pad 3) as found by FEM simulations.

Finally, the total displacement (hydrostatic + deviatoric) is computed by FEM simulations as shown in Fig. 5. It should be noted that these results are based on anisotropic-plastic behavior for Cu and does not account for creep. Therefore, the deformation for the Cu pads exhibiting creep (with E<130 GPa) is underestimated. A clear correlation exists between E and the total deformation where Cu pads with lower E yield larger deformation. Since thermal expansion is orientation-independent in cubic materials, the difference in deformation along Z arises from the difference in deviatoric strain level which was found experimentally to correlate with E and confirmed by FEM simulations.

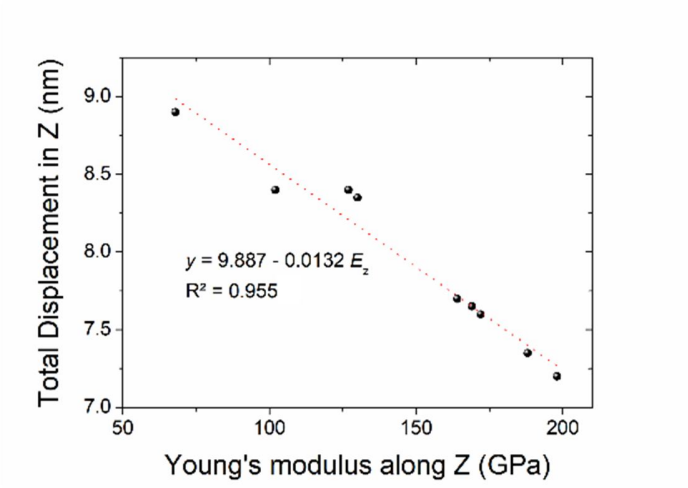

Fig. 5. Total displacement in normal direction to the pad plane vs. Young's modulus as found by FEM simulations.

3.3 Application to Hybrid Bonding

The thermomechanical study of individual Cu pads is of critical interest for the hybrid bonding process of 300 nm monocrystalline Cu pads. In fact, and prior to W2W hybrid bonding, copper dishing (which is the recess of the Hybrid Bonding Metal pad center with respect to the edges) can occur during the Chemical Mechanical Polishing (CMP) step of the two surfaces to be bonded [27][28]. W2W bonding is carried out first at room temperature with weak SiO_2-SiO_2 adhesion. Therefore, annealing is carried out to strengthen the bonding interface and the bonding energy in SiO_2-SiO_2 zones and also Cu-Cu connections. Partial bonding due to large Cu dishing may occur leading to serious mechanical and electrical reliability issues such as (a) a decreasing contact area between the bonding surfaces, leading to debonding at lower loads and (b) generating large initial defects at the interface that are likely to develop towards critical defects due to fatigue, electromigration or stress voiding phenomena.

The results of Fig. 5 show that, depending on the orientation, a difference of 2 nm in displacement can be found for single pads which gives a total of 4 nm in bonding. At this level of Cu pad width, the 4 nm gap is significant [12]. The specifications for Cu dishing should therefore be based on the [111] orientation (E_{max} and minimum deformation) in order to secure full interface closure after hybrid bonding.

4. Conclusions

In conclusion, this paper presents a unique in situ Laue micro-diffraction study of individual 300 nm Cu pads. A clear relationship between their microstructure and their mechanical behavior as a function of temperature up to 400 °C has been established. At smaller pad sizes, the microstructure plays an important role in HB. All Cu pads investigated in this work are monocrystalline with no clear dominant orientation and no orientation change while heating. The crystal deformation is directly related to the crystalline orientation where pads with orientation closer to [100] along the vertical direction deform more easily and therefore exhibit larger deformation upon annealing due to a smaller Young's modulus. The main contributor to the difference in total deformation is linked to the deviatoric strain whereas the hydrostatic strain is similar for all pads. It was further found that pads with E<130 GPa exhibit plastic behavior at temperatures lower than 150 °C and higher than 350 °C. A Ludwick plasticity law was successfully used to fit the experimental results. The plasticity law parameters were extracted for these pads with the help of DoCE revealing a relation between the pad's orientation and thus Young's modulus and Ludwick's parameters. In addition, creep was evidenced during the annealing at 400 °C. This study offers profound and unique understanding of the mechanical behavior of individual sub-micron Cu pads during thermal treatment. It allows us to anticipate a threshold dishing for full bonding for 300 nm HB Cu pads. The minimum dishing is defined with respect to the minimum deformation obtained upon annealing according to the pad closest to the [111] orientation.

Acknowledgments

We acknowledge the European Synchrotron Radiation Facility for provision of synchrotron radiation facilities, and we would like to thank Jean-Sebastien Micha and Samuel Tardif for assistance in using beamline 32.

This work was supported by the French National Research Agency (ANR) under the "Investissements d'avenir" programs: ANR 10-AIRT-0005 (IRT NANO-ELEC) and by the cooperative Research & Development program "IPCEI, Nano 2022".

References

[1] International Roadmap for Devices and Systems™ (IRDS). More Moore. 2021. http://irds.ieee.org/.

[2] P. Garrou, C. Bower and P. Ramm. Handbook of 3D Integration, vols. 1 & 2, Technology and Applications of 3D Integrated Circuits (2012).

[3] G. Taylor, "A method of drawing metallic filaments and a discussion of their properties and uses", Phys. Rev., vol. 23, p. 655, (1924). https://doi.org/10.1103/PhysRev.23.655.

[4] C. Herring and J. K. Galt, "Elastic and plastic properties of very small metal specimens," Phys. Rev, vol. 85, pp. 1060-1061, (1952). https://doi.org/10.1103/PhysRev.85.1060.2.

[5] S. S. Brenner, "Tensile Strength of Whiskers", Journal of Applied Physics 27, pp. 1484-1491, (1956). https://doi.org/10.1063/1.1722294.

[6] A. E. Yarimbiyik, H. A. Schafft, R. A. Allen, M. D. Vaudin and M. E. Zaghloul. "Experimental and simulation studies of resistivity in nanoscale copper films" Microelectronics Reliability, 49(2), pp. 127-134, (2009). https://doi.org/10.1016/j.microrel.2008.11.003.

[7] H. Zahedmanesh, O. Varela Pedreira, C. Wilson, Z. Tőkei, and K. Croes, "Copper electromigration; prediction of scaling limits." Proc. International Interconnect Technology Conference 1 (2019).

[8] H. Ceric, S. Selberherr, H. Zahedmanesh, R. L. de Orio, and K. Croes. "Review — Modeling Methods for Analysis of Electromigration Degradation in Nano-Interconnects. " ECS Journal of Solid State Science and Technology, (2021). https://doi.org/10.1149/2162-8777/abe7a9.

[9] Y. Champion, C. Langlois, S. Guérin-Mailly, P. Langlois, J. L. Bonnentien and M. J. Hÿtch. Near-perfect elastoplasticity in pure nanocrystalline copper. Science, 300(5617), 310-311, (2003). https://doi.org/10.1126/science.1081042

[10] J. Schiøtz, F. Di Tolla and K. Jacobsen. Softening of nanocrystalline metals at very small grain sizes. Nature 391, 561–563, (1998). https://doi.org/10.1038/35328

[11] S. N. Naik and S. M. Walley (2020). The Hall–Petch and inverse Hall–Petch relations and the hardness of nanocrystalline metals. Journal of Materials Science, 55(7), 2661-2681.

[12] C. Sart, S. Estevez, R. Fiori, S. Lhostis, E. Deloffre, G. Parry and R. Gonella, "Cu/SiO_2 hybrid bonding: Finite element modeling and experimental characterization," 2016 6th Electronic System-Integration Technology Conference (ESTC), pp. 1-7, (2016). https://doi.org/10.1109/ESTC.2016.7764484.

[13] T. Tomoyuki. "Work hardening of copper single crystals with multiple glide orientations." Transactions of the Japan Institute of Metals 16.10, pp. 629-640, (1975). https://doi.org/10.2320/matertrans1960.16.629.

[14] J.S. Micha. In https://gitlab.esrf.fr/micha/lauetools/-/tree/master. Last revision : Sept 2021.

[15] Odile Robach, C. Kirchlechner, J.S. Micha, O. Ulrich, X. Biquard, O. Geaymond, O. Castelnau, M. Bornert, J. Petit, S. Berveiller and O. Sicardy, "Laue microdiffraction at the ESRF" In Imperial College Press, pp.156-204, (2014). https://doi.org/10.1142/9781908979636_0005.

[16] J.S. Micha. https://www.esrf.fr/UsersAndScience/Experiments/CRG/BM32/Microdiffraction, Laue Introduction, 2020.

[17] E.J. Hearn, Mechanics of Materials 2 (Third Edition), Chapter 8 - Introduction to Advanced Elasticity Theory, Editor(s): E.J. Hearn, Butterworth-Heinemann, pp. 220-299, (1997).

[18] Y. Okada and Y. Tokumaru, "Precise determination of lattice parameter and thermal expansion coefficient of silicon between 300 and 1500 K." Journal of applied physics 56.2, pp. 314-320, (1984). https://doi.org/10.1063/1.333965.

[19] N. P. Bansal and R.H. Doremus, "Handbook of glass properties." Elsevier, (2013). https://doi.org/10.1016/B978-0-08-052376-7.50004-7.

[20] A. Masolin, P.O. Bouchard, R. Martini and M. Bernacki, "Thermo-mechanical and fracture properties in single-crystal silicon." Journal of Materials Science 48.3, pp. 979-988, (2013). https://doi.org/10.1007/s10853-012-6713-7.

[21] J.F. Nye, "Physical properties of crystals: their representation by tensors and matrices", Oxford university press, (1985).

[22] R.W. Hertzberg, "Deformation and Fracture Mechanics of Engineering Materials", John Wiley & Sons, (1983).

[23] W.D. Callister, Fundamentals of Materials Science and Engineering, 2nd ed., p.169, (2005).

[24] C. Sart, “Numerical and experimental investigations on mechanical stress in 3D stacked integrated circuits for imaging applications,” Ph.D. dissertation, Grenoble, France, (2019).

[25] R.P. Vinci, E.M. Zielinski, and J.C. Bravman, "Thermal Stresses in Passivated Copper Interconnects Determined by X-Ray Analysis and Finite Element Modeling", MRS Proceedings 338, (1994). https://doi.org/10.1557/PROC-338-289.

[26] M.A. Marcus, W.F. Flood, R.A. Cirelli, R.C. Kistler, N.A. Ciampa, W.M. Mansfield, D.L. Barr, C.A. Volkert and K.G. Steiner, "X-Ray Strain Measurements in Fine-Line Patterned AL-CU Films", MRS Proceedings 338, (1994). https://doi.org/10.1557/PROC-338-203.

[27] J.J. Vlassak, "A model for chemical–mechanical polishing of a material surface based on contact mechanics", Journal of the Mechanics and Physics of Solids, Volume 52, Issue 4, Pages 847-873, (2004). https://doi.org/10.1016/j.jmps.2003.07.007.

[28] G. Fu and A. Chandra, "An analytical dishing and step height reduction model for chemical mechanical planarization (CMP)," in IEEE Transactions on Semiconductor Manufacturing, vol. 16, no. 3, pp. 477-485, (2003). https://doi.org/10.1109/TSM.2003.815202.